Title

Developing Metal-Binding Isosteres of 8-Hydroxyquinoline as Metalloenzyme Inhibitor Scaffolds

Journal

Inorganic Chemistry, 61(19)

ISSN

0020-1669

Authors

Seo, Hyeonglim
Jackl, Moritz K
Kalaj, Mark
et al.

Publication Date

2022-05-16

DOI

10.1021/acs.inorgchem.2c00891

Peer reviewed

HHS Public Access

Author manuscript

Inorg Chem. Author manuscript; available in PMC 2023 February 10.

Published in final edited form as:

Inorg Chem. 2022 May 16; 61(19): 7631–7641. doi:10.1021/acs.inorgchem.2c00891.

Developing Metal-binding Isosteres of 8-Hydroxyquinoline as Metalloenzyme Inhibitor Scaffolds

Hyeonglim Seo,

Moritz K. Jackl,

Mark Kalaj,

Seth M. Cohen*

Department of Chemistry and Biochemistry, University of California, San Diego, La Jolla, California, 92093, USA

Abstract

The use of metal-binding pharmacophores (MBPs) in fragment-based drug discovery (FBDD) has proven effective for targeted metalloenzyme drug development. However, MBPs can still suffer from pharmacokinetic liabilities, such as poor solubility and low membrane permeability. Bioisostere replacement is an effective strategy utilized by medicinal chemists to navigate these issues during the drug development process. The quinoline pharmacophore and its bioisosteres, such as quinazoline, are important building blocks to modulate drug-target interactions and physicochemical properties in the design of new therapeutics. More relevant to metalloenzyme inhibition, 8-hydroxyquinoline (8-HQ) and its derivatives can serve as MBPs for metalloenzyme inhibition. In this report, 8-HQ isosteres are designed and the coordination chemistry of the resulting metal-binding isosteres (MBIs) is explored using a bioinorganic model complex. In addition, the physicochemical properties and metalloenzyme inhibition activity of these MBIs were investigated to establish drug-like profiles. This report provides a new group of 8-HQ-derived MBIs that can serve as novel scaffolds for metalloenzyme inhibitor development with tunable, and potentially improved, physicochemical properties.

Graphical Abstract

***Corresponding Author**: scohen@ucsd.edu (S.M.C.).

The authors declare the following competing financial interest(s): S.M.C. is a co-founder, has an equity interest, and receives income as member of the Scientific Advisory Board for Forge Therapeutics; is a co-founder, has an equity interest, and is a member of the Scientific Advisory Board for Blacksmith Medicines; and is a co-founder and has an equity interest Cleave Therapeutics (formerly Cleave Biosciences). These companies may potentially benefit from the research results of certain projects in the laboratory of S.M.C. The terms of this arrangement have been reviewed and approved by the University of California, San Diego in accordance with its conflict of interest policies.

Supporting Information. The Supporting Information is available free of charge on the ACS Publications website at DOI: xx. Crystal data tables, synthetic procedures, characterization data, and supplementary figures and tables.

Accession Codes. CCDC 2123145–2123170 contain the supplementary crystallographic data for this paper. These data can be obtained free of charge via www.ccdc.cam.ac.uk/data_request/cif, by emailing data_request@ccdc.cam.ac.uk, or by contacting The Cambridge Crystallographic Data Centre, 12 Union Road, Cambridge CB2 1EZ, UK; fax: +44 1223 336033.

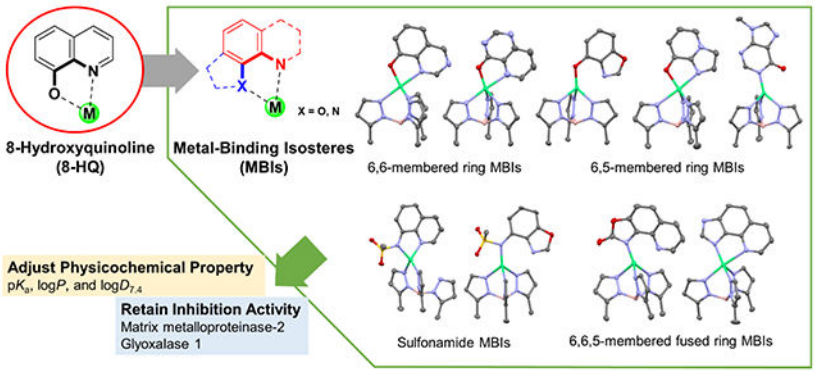

Keywords

metalloenzyme inhibitor; fragment-based drug discovery; metal binding isosteres; bioisosteres; 8-hydroxyquinoline

INTRODUCTION

Metalloenzymes are involved in numerous biological processes and are important therapeutic targets to treat a wide range of diseases including cancer, neurological disorders, and viral infections.[1] The majority of FDA-approved metalloenzyme inhibitors coordinate to the catalytic active site metal ion via a metal-binding pharmacophore (MBP), which has been evidenced by numerous crystallographic studies of metalloenzyme inhibitors in complex with their protein targets.[1] However, among these clinically used metalloenzyme inhibitors, a limited number of MBPs have been employed to bind active site metal ions, with an overreliance on carboxylic acid, hydroxamic acid, and a handful of other MBPs. To overcome this limited chemical space for MBPs, efforts have been made to development fragment libraries to broaden the scope of MBPs available for lead development.[2] Nonetheless, these and other commonly investigated MBPs can suffer from pharmacokinetic liabilities such as metabolic instability, poor solubility, and low membrane permeability (e.g., hydroxamic acid)[2] that ultimately limit the usefulness of many MBPs as lead scaffolds for the development of effective therapeutics.

To facilitate the development of metalloenzyme inhibitors, isosteric replacement of MBPs has been performed to produce metal-binding isosteres (MBIs). Isosteric replacement involves replacing functional groups that can result in adverse physicochemical properties with less detrimental groups that retain biological activity.[3,4] As a result, MBIs combine the metal-binding features of MBPs with the principle of isosterism to expand chemical diversity and improve pharmacokinetic liabilities. MBIs can then be used as fragments for fragment-based drug discovery (FBDD) campaigns directed at metalloenzymes. For example, picolinic acid MBIs have been studied by performing isosteric replacements of the carboxylic acid and the pyridine ring and their metal-binding ability, electronic properties, physicochemical properties, and biological activities were investigated.[5–7] These studies showed that MBIs are a viable strategy to provide new metal-binding functional groups for metalloenzyme inhibition.

8-Hydroxyquinoline (8-HQ) is a common scaffold found in bioactive small molecules and drugs, and has been used for iron-chelation for neuroprotection, anticancer activity, anti-HIV activity, and antifungal activity.[8, 9] Additionally, this motif has been applied as an MBP for metalloenzymes inhibitors including matrix metalloproteinases,[10, 11] 2-oxoglutarate (2OG)/Fe(II) dependent oxygenases,[12, 13] and aminopeptidase from *Aeromonas proteolytica* (AAP).[14] For example, 5-carboxy-8-hydroxyquinoline was reported as a potent broad-spectrum inhibitor of the 2OG oxygenases including JmjC demethylases. However, like many MBPs, 5-carboxy-8-hydroxyquinoline suffers from low cell permeability.[12] Furthermore, the propensity of underivatized 8-HQ to bind several different metalloenzymes can lead to undesirable off-target interactions. Indeed, various strategies, including functionalization of the molecule, molecule hybridization, and glycoconjugation have been performed to improve the selectivity and decrease toxicity of a broad range of 8-HQ-based drug candidates.[15–17] However, modifications of the core 8-HQ scaffold has not been widely studied in the context of metalloenzyme inhibitor development and it is unknown how changes to the molecular structure of 8-HQ will influence important parameters such as metal-binding ability and physicochemical properties.

Herein, a novel MBI library of isosteres of 8-hydroxyquinoline (8-HQ) was designed, synthesized, and characterized. In total, 30 MBIs of 8-HQ were prepared focusing on nitrogen heterocycle replacements with various ring systems. The 8-HQ MBIs described here can be categorized into four broad groups: 6,6-membered ring MBIs, 6,5-membered ring MBIs, sulfonamide MBIs, and 6,6,5-membered fused ring MBIs. Their physicochemical profiles (pK_a and $\log D_{7.4}$) were explored to gain insights about their electron donor ability and pharmacological properties. The metal-binding of the MBIs was studied using a bioinorganic model system and compared to the parent 8-HQ compound. Furthermore, the inhibition activities of MBIs against representative metalloenzymes were determined.

RESULT AND DISCUSSION

Library Design and MBI Synthesis.

8-Hydroxy quinoline (8-HQ) binds to transition metal ions through its oxygen and nitrogen donor atoms.[18] In the design of 8-HQ MBIs, the 5-membered chelate ring of the ligand bound to the metal was retained in the MBI design and selection. Two parts of the molecule, the quinoline ring and the hydroxyl group, were investigated for isosteric replacement (Figure 1). First, several different aromatic heterocyclic replacements were carried out on the quinoline ring by varying ring sizes and adding heteroatoms. The heterocyclic cores of the potential MBIs were evaluated using DrugBank[19] to find drug-like fragments, which is a drug database that includes FDA-approved small-molecule drugs, as well as experimental drugs. Indole, purine, benzimidazole, and quinazoline were found as common substructures in the DrugBank database (>120 small molecules, Table S1). These nitrogen heterocycles are widely used as scaffolds in drug discovery and are common motifs in FDA-approved drugs.[20, 21] Including these four scaffolds, 14 aromatic heterocycles were also considered for use as quinoline isosteres based on their structural similarity and synthetic accessibility (Table S1). For the hydroxyl group replacements, sulfonamide, carbamate,

carbamide, imidazole, and triazole groups were utilized. Combined, this produced a library consisting of 30 MBIs in total (Figure 1). Importantly, although some of these compounds, or substructures of these compounds have been reported to have biological activity,[22–27] their use as a metal-binding scaffolds in metalloenzyme inhibitors have not been extensively investigated. Indeed, a search of the Cambridge Crystallographic Data Centre (CCDC) shows that even the fundamental coordination chemistry of most molecules described in this study have not been described. For example, while >2300 structures containing 8-HQ bound to metals are available in the CCDC, few structures of 8-HQ MBIs have been described and at least 20 of the MBIs reported here have no entries of metal complexes in the CCDC (Table S2).

MBIs **1**, **3**, **4**, **5**, **7**, **9**, **10**, **11**, **13**, **14**, **15**, and **17** were purchased from commercial vendors, while the remaining MBIs synthesized from widely available starting materials. MBIs **2**, **6**, **16**, and **25** – **30** were synthesized based on annulation reactions using commercially available starting materials. MBI **8** was prepared through methylation and deprotection of an *O*-benzyloxy-protected benzimidazole. MBI **12** was synthesized by deprotection of an *O*-benzyloxy-protected indole. MBIs **18** – **24** were prepared by the reaction of anilines with methyl sulfonyl chloride. The detailed synthetic procedures and the complete characterization of all synthesized MBIs can be found in the Supporting Information.

Physicochemical Properties Analysis.

Physicochemical properties (pK_a and log$P$) of MBIs were measured using UV-based or potentiometric methods using a SiriusT3 apparatus (Table 1).[28–30] Log$D_{7.4}$ values were derived from measured pK_a and log$P$ and log$D_{7.4}$ values were used to gauge the lipophilicity of MBIs (Table 1). In general, for pK_a values of 8-HQ MBIs, there are two values in the range of pH 2.0 – 12.0. The first value (pK_{a1}) is related to the conjugated acid (protonated nitrogen) of the heteroaromatic ring system and the second value (pK_{a2}) corresponds to the hydroxyl group or its isosteric replacement (Table 1). Overall, a broad range of acidities (pK_{a1} = 2.16 – 5.43, pK_{a2}= 3.34 – 11.75) and lipophilicities (log$D_{7.4}$=−3.83 – 1.97) were measured for the MBIs.

Physicochemical properties of 6,6-membered ring MBIs (MBIs **1** – **5**) were modulated by the presence of nitrogen atoms in the ring structure. This change was reflected in the acidity and the lipophilicity of the MBIs. Specifically, MBIs containing more nitrogen atoms had lower pK_a values indicating an increase in the acidity of the hydroxyl groups and a decrease in the basicity of the nitrogen atoms of the ring systems. In addition, significantly lower log$D_{7.4}$ values were observed when more nitrogen atoms were added to the ring system. For example, MBI **5**, which contains the most nitrogen atoms in the ring system, showed the lowest pK_a and log$D_{7.4}$ values in this group.

In the case of 6,5-membered ring MBIs (MBIs **6** – **17**), higher pK_{a1} values were observed for MBIs **8**, **9**, and **10**. These findings suggest that the heteroaromatic nitrogen atoms of MBIs **8**, **9**, and **10** are more basic compared to the other 6,5-membered rings. In general, the lipophilicity decreased as more heteroatoms are added to the ring system. Interestingly, this

was not observed for MBI **7** containing the benzothiazole scaffold – the lipophilicity of this MBI was almost identical to 8-HQ (log$D_{7.4}$ = 1.84 for MBI **7** vs 1.85 for 8-HQ).

When the hydroxyl groups are replaced with sulfonamides (MBIs **18** – **24**), both pK_a values slightly decreased. However, similar trends shown in the above MBIs were observed for the sulfonamide MBIs. The nitrogen ring count in the aromatic system decreases the pK_a values (MBIs **18** – **20**) and certain scaffolds (MBIs **23** and **24**) show relatively high pK_{a1} values. The benzothiazole scaffold (MBI **22**) significantly increases lipophilicity and indicates the highest log $D_{7.4}$ value in the sulfonamides MBIs (log$D_{7.4}$ = 1.16 for MBI **22**).

In 6,6,5-membered fused ring MBIs (MBIs **25** – **30**), MBI **29** have the highest pK_a values, which indicates that this MBI has the most basic nitrogen in this group. Log$D_{7.4}$ values of these MBIs (log$D_{7.4}$ = 1.23 to 1.97) were comparable to 8-HQ (log$D_{7.4}$ = 1.85). MBI **26** was an exception (log$D_{7.4}$ = 0.22), which can be explained with its stronger acidity (pK_{a2} = 6.45) compared to the other three-fused rings – at physiological pH a significant amount of MBI **26** is deprotonated, which decreases lipophilicity. The results demonstrate that important physicochemical properties can be optimized by isosteric replacements.

Structural Analysis.

[Tp^{Ph,Me}Zn(**MBI**)] (Tp^{Ph,Me} = hydrotris(5,3-methylphenylpyrazolyl)borate) complexes were prepared as a model system to gain an understanding about the metal-binding ability and coordination chemistry of the MBIs. [Tp^{Ph,Me}Zn(OH)] complex and its derivatives have been broadly used to mimic the tris(histidine) Zn(II) active site of many metalloenzymes (e.g., carbonic anhydrase or matrix metalloproteinases).[31–33] [Tp^{Ph,Me}Zn(**MBI**)] complexes of 6,6-membered ring MBIs (8-HQ and MBIs **1** – **5**) were prepared and analyzed by X-ray crystallography (Figure 2). These MBIs coordinate to the Zn(II) center in a bidentate fashion via the nitrogen atom of the aromatic ring system and the deprotonated hydroxyl group. All complexes generated trigonal bipyramidal geometries with the structural parameter τ_5 in a similar range (τ_5 = 0.67 - 0.73, τ_5 = 0; square pyramidal geometry, τ_5 = 1; trigonal pyramidal geometry). [Tp^{Ph,Me}Zn(**1**)] containing quinazoline is most similar to [Tp^{Ph,Me}Zn(8-HQ)] based on their structural similarities (Table 2). Interestingly, while the Zn-O bond lengths were comparable for most MBIs, there was a significant difference in the bond lengths of MBI Zn-N distance depending on the ring scaffold. For example, MBI **5**, which has the highest nitrogen atom count, showed the largest increase in Zn-N bond length, with a Zn-N bond length 0.2 Å longer than the Zn-N bond in the 8-HQ complex (Table 2). This corresponds to the basicity of MBI **5** (pK_{a1} < 2) and 8-HQ (pK_{a1} = 4.97) and suggests that the donor ability of the nitrogen donor is reduced as the number of nitrogen atoms in the aromatic ring system increases.

Next, [Tp^{Ph,Me}Zn(**MBI**)] model complexes of 6,5-membered ring MBIs (MBIs **6**, **7**, **8**, **9**, **11**, **13**, and **16**) were studied (Figure 3). In general, these MBIs showed a larger variety of binding modes compared to the 6,6-membered ring MBIs. MBI **6** and **11** coordinate to the Zn(II) center in a monodentate fashion with the deprotonated hydroxyl group while MBI **7**, **8**, and **9** showed bidentate binding to the Zn(II) ion through the oxygen and nitrogen. This could be explained by stereo-electronic effects. For MBIs **6** and **11**, exchanging the

6-membered pyridine ring of 8-HQ for a 5-membered oxazole/pyrazole ring positions the oxygen and nitrogen donor atoms in a geometry that produces unfavorable bite-angles when bound to a metal. For example, MBIs **6** and **11** have the largest value in angle **a** (Figure 3), which is one of the angles that makes up the 5-membered chelate ring (~130° for MBIs **6** and **11** vs. ~116 ° for 8-HQ, Table 3). In addition, the NH group in the pyrazole ring of MBI **11** is predominantly located at N1 based on the X-ray structure, which would preclude a bidentate binding mode (Figure 3). In contrast, the thiazole ring in MBI **7** leads to a better geometry of the oxygen and nitrogen donor atoms for bidentate coordination. Due to the lack of hybridization of the sulfur atom, the thiazole ring is distorted, which "squeezes" the oxygen and nitrogen donor atoms in a geometry more like 8-HQ, resulting in a bidentate binding mode (see angles designated **a** and **b** in Figure 3, Table 3). MBIs **8** and **9** have potentially better nitrogen donors based on their higher basicity (pK_{a1} = 4.61 and 5.43, Table 1) compared to other 6,5-membered ring MBIs (pK_{a1} of MBI **6**, **7**, and **11** < 2, Table 1), which could compensate for the unfavorable bite-angle and explain the bidentate binding modes. Another interesting set of MBIs was purine or pyrimidine-based scaffolds (MBI **13** – **16**). Figure 3 shows that MBI **13** and **16** provided monodentate coordination to the Zn(II) center through N1. This finding is explained by metal-binding patterns in the anionic form of purine or pyrimidine-based nucleobases such as guanine and thymine.[34, 35] Those nucleobases are known to be deprotonated at N1 and metal-bindings then take place through the deprotonated N1 site.[36–40]

The [Tp^{Ph,Me}Zn(**MBI**)] complexes with sulfonamide series (MBI **18** – **24**) exhibited similar binding behavior as the hydroxyl series discussed above with a few exceptions (Figure 4). 6,6-Membered sulfonamide rings (MBIs **18** – **20**) coordinate to the Zn(II) ion in a bidentate fashion. Interestingly, MBIs **18** and **19** resulted in a complex where one pyrazole of the Tp^{Ph,Me} ligand was displaced from the metal center resulting in a tetrahedral geometry (τ_4 = 0.81 - 0.85, τ_4 = 0; square planar geometry, τ_4 = 1; tetrahedral geometry, Table S5). Pyrazole displacement in these model systems has been previously observed in rare cases,[5, 41] but this remains a rare observation in these systems. In this case, this could indicate the ability of these MBIs to have a greater perturbation to the active site of a metalloenzyme upon binding. This may also be relevant to the use of 8-sulfonamidoquinoline and its derivatives as biological Zn(II) sensors, metal chelators, and ionophores.[42–45] For 6,5-membered sulfonamide rings, monodentate (MBI **21**) and bidentate binding modes (MBIs **23** and **24**) were found with the [Tp^{Ph,Me}Zn(**MBI**)] system. Note that the nitrogen atoms of MBI **23** and **24** (pK_{a1} = 4.45 and 4.56, Table 1) are more basic compared to MBI **21** (pK_{a1} <2), which potentially translates to a stronger donor ability to the metal center. The improved donor ability of benzoimidazole and imidazopyridine scaffolds was also observed for the 6,5-membered hydroxyl substituted MBIs (**8** and **9**, see above). All attempts to prepare [Tp^{Ph,Me}Zn(**22**)] resulted in a neutral, homoleptic complex where two ligands coordinate to a single Zn(II) ion ([Zn(**22**)$_2$], Figure S1). This result was rather surprising, as prior studies have indicated it is extremely uncommon that an MBI will strip the Zn(II) ion from the Tp^{Ph,Me} spectator ligand.[5, 6] Strong affinity toward Zn(II) or unanticipated reactivity with the [Tp^{Ph,Me}Zn(OH)] complex could explain the observed metal stripping phenomenon of MBI **22**. MBI **22** is a previously unreported compound and further studies will be required to elucidate its reactivity and affinity toward Zn(II) to explain the unusual behavior seen

here. Overall, the results demonstrated that sulfonamide functionalization can be considered a good strategy for efficient metal-binding isosteric replacement of 8-HQ.

Lastly, [$Tp^{Ph,Me}$Zn(**MBI**)] model complexes of the 6,6,5-membered fused ring MBIs were prepared and their binding behavior was investigated (Figure 5). Surprisingly, except for MBI **29**, all MBIs bound the metal in a monodentate binding mode. This indicates that the rigid backbone of these MBIs pre-arranges the donor atoms in a geometry that would result in unfavorable bite angles. For example, angle **a** of the 6,6,5-membered fused ring MBIs was at least 10° greater (~127 – 130°, Figure 5, Table 4) than the corresponding angle of the 8-HQ (~116°). Consequently, monodentate binding is favored and few bidentate binding modes are observed for these compounds. MBIs **25**, **27**, **28**, and **30** bind to the Zn(II) center via the deprotonated nitrogen atoms (labeled N1, Figure 5) of the carbamate, carbamide, and tetrazole. MBI **25** was specifically designed to try to enforce bidentate binding by the arrangement and substitution of the heteroatoms in the 5-membered ring; indeed, these complexes, although possessing 4-coordinate Zn(II) centers show a strongly distorted geometry with Zn-N2 distances of 2.62 (Table 4). MBI **26** binds to the metal center with a negatively charged sulfur atom formed by deprotonation of the thiocarbamate moiety. A possible explanation for the metal-binding behavior could be that sterically restrained 6,6,5-fused rings decreases its coordination ability and iminothiolate could act as a dominant metal-binder as a result of tautomerization of the thiocarbamate upon deprotonation.[46] As mentioned previously, MBI **29** was the only compound exhibiting bidentate coordination. This may be explained by the increased donor ability of the imidazole nitrogen atom found in MBI **29**, which is reflected in the relatively high pK_a values compared to other MBIs in this subgroup (pK_{a1} and pK_{a2} of MBI **29** = 4.92 and 11.75, Table 1). As described above, a correlation between metal-binding behavior and basicity is observed for many of the other 8-HQ MBIs. Presumably, the increased donor ability compensates for the unfavorable bite-angle caused by steric constraints, resulting in a bidentate binding mode. In summary, the comprehensive structural analysis on 8-HQ MBIs in the [$Tp^{Ph,Me}$Zn(**MBI**)] model complex not only shed light on the effect of different isosteric replacements on the coordination chemistry of each MBI (i.e., ligand basicity, bond angle/orientation, donor atom identity, and tautomerization), but also presented potentially useful MBIs with various metal-binding modes.

MBI Screening.

To evaluate 8-HQ MBIs as potential fragment scaffolds for metalloenzyme inhibitors, the inhibitory activity of these MBIs against three Zn(II)-based metalloenzymes was measured. Matrix metalloproteinase-2 (MMP-2) and human glyoxalase 1 (GLO1) were selected as these enzymes are known to be inhibited by 8-HQ.[10, 11, 47] Human carbonic anhydrase II (hCAII) is another Zn(II)-based metalloenzyme that was tested in this study. There is no significant inhibitory activity reported for 8-HQ against hCAII and thus selectivity of the 8-HQ MBI library was evaluated with this enzyme. Both MMP-2 and hCAII contain a catalytic Zn(II) ion coordinated by three histidine residues and a water molecule in a tetrahedral geometry.[48, 49] In GLO1, the Zn(II) ion is coordinated to Gln33, Glu99, His126, and Glu172 in an octahedral coordination geometry with two open coordination sites occupied by exchangeable water molecules.[50] It has been reported that the nitrogen

and the hydroxyl oxygen donor atoms of 8-HQ bind to the catalytic Zn(II) ion in MMP-2 and GLO1 resulting in inhibition.[10, 11, 47] To validate this hypothesis, the inhibition activity of compounds **31** and **32**, as well as 8-HQ were measured against MMP-2 and GLO1 at a concentration of 200 μM (Table 5). Compound **31** replaces the pyridine nitrogen donor atom with a poor dimethylamino ligand. Compound **32** moves the hydroxyl group to the 6-position of the quinoline scaffold resulting in an inability to produce bidentate binding. Unsurprisingly, the inhibition activity of **31** and **32** against MMP-2 and GLO1 was reduced by >50% compared to 8-HQ, suggesting the importance of metal binding to inhibit these enzymes (Table 5). All the 8-HQ MBIs were screened at a fragment concentration of 200 μM. The percent inhibition activity of each MBI is shown in Table 5.

The screening result show that MMP-2 is more effectively inhibited by the 6,6-membered ring MBIs. While the 6,6-membered ring MBIs **1** – **3** and **5** showed moderate inhibition (30 – 40% at 200 μM), the 5,6-membered ring MBIs **6** – **16** were nearly inactive. These results confirm previous studies on the development of MMP-2 inhibitors based on 8-sulfonamido quinoline derivatives and its 5,6-membered heterocycle isosteres.[51, 52] MBIs **1** – **3** and **5**, which have more nitrogen atoms in the ring system, showed a poorer IC_{50} value than 8-HQ (Figure S2), suggesting that adding nitrogen atoms to the core scaffold does not enhance interaction with the binding pocket. On the other hand, sulfonamide MBI **18** showed modest improvements in inhibition activity compared to 8-HQ (IC_{50} of MBI **18** = 153.6±9.8 μM, IC_{50} of 8-HQ = 165.7+12.4 μM, Figure S2). Placing nitrogen atoms on the core scaffold (MBIs **19** and **20**) did not improve inhibition activity as observed in MBIs **1** – **3** and **5**. Interestingly, MBI **26** showed much higher inhibition activity compared to the other 6,6,5-membered fused ring MBIs, presumably due to the high affinity of sulfur for zinc. The moderate inhibition activity of MBI **26** was confirmed by measuring its IC_{50} value (Figure S2). Compounds **33** and **34** were additionally screened to validate the metal binding interaction of MBIs **1** and **18** with MMP-2. Compound **33** has a methyl group on the hydroxyl oxygen atom when compared to MBI **1,** and compound **34** contains a reverse sulfonamide group when compared to MBI **19**. Not surprisingly, both compounds **33** and **34** are not effective inhibitors of MMP-2.

More than half of the 8-HQ MBIs showed significant inhibition activity against GLO1 at a fragment concentration of 200 μM. In general, 6,6-membered ring MBIs **1**, **2**, **18**, **19**, and **20** showed inhibition (>37% at 200 μM) and maintained activity at a lower fragment concentration (>21% at 50 μM, Table S6). Importantly, many 6,5-membered MBIs (MBIs **6** – **13** and **24**), which did not show significant inhibition of MMP-2, showed moderate inhibition against GLO1. Based on the X-ray data obtained for the model complexes, replacing 6,6-membered rings with 6,5-membered ring MBIs produced a greater variety in metal-binding modes and orientations. It is possible that the active site of GLO1 is less susceptible to those changes in metal-binding. Note that indazole-based MBI **11** showed the highest inhibition activity (77% at 200 μM) among the 6,5-membered ring MBIs, and MBIs **9** and **24** containing imidazopyridine core exhibited potent inhibition of GLO1 (41% and 60% at 200 μM, respectively). These findings suggest that these 8-HQ MBIs could be applied as selective fragments for the development of GLO1 inhibitors. In addition, the inhibition activity of compounds **33** and **34** were compared with MBI **1** and **18**, which

showed the highest percent inhibition (>95% at 200 μM). Compound **33** showed a modest decrease in inhibition activity while compound **34** exhibited a complete loss of inhibition. Finally, as an orthogonal method to evaluate MBI binding with GLO1, thermal shift assays (TSAs) were carried out on five select compounds (8-HQ, **1**, **18**, **19**, and **20**, Table S7). The TSA data was reported as ΔT_M (in °C), which refers to the difference in melting temperature of MBI-bound GLO1 compared to native, unbound GLO1. Significant ΔT_M values (>3 °C) were observed for all test compounds, providing independent validation of a binding interaction between these select MBIs and GLO1.

In contrast to MMP-2 and GLO1, only few MBIs showed inhibition activity against hCAII. MBI **12** showed the greatest inhibition of hCAII (89% at 200 μM). TSA data verified binding of **12** with hCAII, showing a significant ΔT_M value (ΔT_M = 7.28±0.18 °C, Table S7). Why MBI **12** is an effective inhibitor of hCAII is not obvious; a possible explanation could be that the indole group interacts with the zinc-coordinated water molecule, which was suggested by molecular docking studies of indole-containing compounds in hCAII.[53] Moreover, a series of benzenesulfonamide derivatives including the indole moiety have been reported with an effective inhibitory activity against hCAII.[54] Interestingly, compound **34** did not show any inhibition activity against hCAII, which is surprising because sulfonamides are privileged scaffolds for hCAII inhibition.[55, 56] The lack of hCAII inhibition by compound **34** may be due to the narrow and deep shape of the hCAII active site.[49]

CONCLUSIONS

In this work, we designed and prepared 30 MBIs derived from 8-HQ that covered a wide range of physiochemical properties. The correlation between electron donor ability of the MBI and ligand basicity were observed based on the pK_a measurement and X-ray crystallography of an [($Tp^{Ph,Me}$)Zn(MBI)] model system. In addition, we confirmed that other factors such as ring scaffold geometry, donor atom identity, bond angle/orientation, and ligand tautomerization can have a pronounced effect on their coordination ability and metal-binding modes. This in-depth analysis allows us to gain better understanding of structural and electronic features of the MBIs and establish a rudimentary rule for future MBI development. Furthermore, bioactivity of the MBIs was monitored by measuring enzymatic activity against several metalloenzymes. The results indicated that the MBIs have comparable potency and improved selectivity, which demonstrates the potential use of 8-HQ MBIs as starting points for the discovery of novel lead candidates in developing metalloenzyme inhibitors. In all, this work demonstrates the utility of bioisosterism to metalloenzyme inhibition, results in the discovery of new ligands, and provides a greater platform for the discovery of a new therapeutics that target metalloenzymes.

EXPERIMENTAL SECTION

General Information.

All reagents and solvents were obtained from commercial sources (Sigma Aldrich, Alfa Aesar, TCI, Combi-Blocks etc.) and used without further purification. 8-Hydroxyquinoline, MBIs **1**, **3**, **4**, **5**, **7**, **9**, **10**, **11**, **13**, **14**, **15**, and **17** were purchased from commercial vendors, and the remaining were synthesized from widely available starting materials. Detailed

synthesis of each MBI is provided in the electronic Supporting Information. Absorbance and fluorescence activity assays were carried out using a BioTek Synergy HT or H4 plate reader.

Synthesis and Crystallization of Model Complexes.

To obtain an X-ray structure of [($Tp^{Ph,Me}$)Zn(MBI)], [($Tp^{Ph,Me}$)K] and [($Tp^{Ph,Me}$)ZnOH] was prepared according to literature methods.[57] [($Tp^{Ph,Me}$)ZnOH] (50 mg, 0.09 mmol) was dissolved in 15 mL of CH_2Cl_2 in a 50 mL round-bottom flask. The MBI (0.09 mmol, 1 equiv) in 10 mL of MeOH was added, and the reaction mixture was stirred overnight under a nitrogen atmosphere. The resulting mixture was evaporated to dryness and subsequently dissolved in a minimal amount (~1 mL) of benzene. The solution was filtered using a syringe filter to remove any undissolved solids. The resulting complex in benzene was recrystallized using vapor diffusion with pentane. Crystals typically formed within a few days.

Physicochemical Properties Analysis.

Physicochemical properties were determined using a Sirius T3 instrument.[29, 58, 59] All titrations, both pK_a and logP, were performed in 0.15 M KCl with 0.5 M HCl and KOH. The pK_a of a compound was determined by analysing each MBI sample in triplicate using potentiometric titrations. Experiments were typically performed over a pH range of 2.0 – 12.0. Standard deviations were derived from fitting all three replicate experiments. For water insoluble compounds methanol was added and the obtained apparent pK_a (p_sK_a) was extrapolated to the aqueous pK_a by the Yasuda-Shedlovsky procedure.[60] LogP was determined via potentiometric titrations in the presence of varying ratios of octanol and water. The presence of octanol shifts the pK_a of ionizable species, and based on the shifts, a logP can be determined. Measurements for logP determination were typically performed over a pH range of 2.0 – 12.0. Three experiments with varying ratios of water:octanol was performed, allowing for a standard deviation to be determined from the fitting of all measurements. MBI sample sizes were ~0.5 mg for both pK_a and logP measurements.

MMP-2 Assay.

Human recombinant MMP-2 catalytic domain was purchased from ENZO Life Sciences (catalog # BML-SE237-0010). Assays were carried out in clear Costar 96-well, half-area, flat-bottom assay plates (catalog # 80-2404). Each well contained a total volume of 100 μL including buffer (50 mM MES, 10 mM $CaCl_2$, 0.05% Brij-35, pH 7.5), MMP-2 (1.16 U), and the fragment solution (200 μM final concentration). After a 30 min incubation period at 37 °C, the reaction was initiated by the addition of 10 μL of fluorogenic MMP-2 substrate (4 μM final concentration, Mca-Pro-Leu-Gly-Leu-Dpa-Ala-Arg-NH2·AcOH, ENZO Life Sciences, catalog # BML-P126-0001). Fluorescence was monitored at E_x/E_m=328/420 nm using BioTek Synergy H4 plate reader, and measurements were recorded every minute for 10 min. The rate of fluorescence increase was compared for samples versus negative controls (no inhibitor, arbitrarily set as 100% activity). A positive control (NNGH as inhibitor, 50 μM final concentration) showed complete inhibition under the assay conditions described above. Dose-response curves were generated, analyzed, and fitted to obtain IC_{50} values of MBIs using a concentration range of between 10 μM and 1000 or 1500 μM

depending on compound solubility (Figure S2). 8-HQ gave an IC_{50} value of 165.7 ± 12.4 μM, which is comparable to the literature reported value (130 ± 28 μM).[10]

GLO1 Assay.

Recombinant human glyoxalase I (GLO1) was purchased from R&D Systems (catalog #4959-GL). Assays were carried out in 0.1 M sodium phosphate, pH 7.0 buffer, utilizing 96-well clear UV plates (Corning UV Transparent Microplates, catalog #3635). A fresh solution of GSH (100 mM) and methylglyoxal (MG) (100 mM) was prepared in Millipore grade water. The substrate for the assay was prepared by adding 0.43 mL of GSH and 0.43 mL of MG to 15.14 mL of buffer. The substrate mixture was vortexed vigorously for 45 s and then allowed to sit at room temperature for 15 min. The initial well volume was 50 μL containing GLO1 (40 ng) and inhibitor. This protein and inhibitor mixture was incubated for 15–20 min prior to addition of the substrate. The substrate (150 μL) was then added to the wells yielding a maximum amount of 5% DMSO per well. The enzyme activity was measured utilizing a Biotek Synergy HT plate reader by measuring absorbance at 240 nm every 1 min for a duration of 8 min. The rate of absorbance increase was compared for samples versus controls containing no inhibitor (set at 100% activity). The absorbance reading for background wells containing DMSO, buffer, and substrate (no enzyme or inhibitor) was subtracted from the experimental wells. A positive control (Chugai-3d inhibitor, 50 μM final concentration) showed complete inhibition under the assay conditions described above.[61]

hCAII Assay.

The plasmid for recombinant expression of hCAII with a T7 RNA polymerase promoter and ampicillin resistance gene (pACA) was a gift from Thomas R. Ward (U. Basel, Switzerland). The protein for activity assays was expressed in BL21 Escherichia coli cells and purified as reported previously.[62] The Zn(II) content of expressed hCAII was measured by inductively coupled plasma-mass spectrometry (ICP-MS). The metal-to-protein (Zn:protein) molar ratio was determined to be 0.951±0.006, indicating the holo enzyme (fully metalated) is was isolated (data not shown). Assays were carried out in clear-bottom Costar 96-well plates (catalog # 07-200-706) with a total volume of 100 μL per well. The assay buffer was comprised of 50 mM HEPES pH 8.0 and 100 mM $NaSO_4$. MBIs were added from a 50 mM DMSO stock to a final concentration of 200 μM and incubated with hCAII (40 nM final concentration) for 15 min at room temperature. *p*-Nitrophenyl acetate was used as the substrate (500 μM final concentration), and the absorbance at 405 nM was monitored for 20 min at 1 min intervals using BioTek Synergy H4 plate reader. Percent inhibition was determined by comparing the activity of wells. A positive control (acetazolamide inhibitor, 50 μM final concentration) showed complete inhibition under the assay conditions described above.

Supplementary Material

Refer to Web version on PubMed Central for supplementary material.

ACKNOWLEDGMENT

This work was supported by the National Institute of Health (R01 AI149444). Financial support for M.K.J. was provided by the Swiss National Science Foundation (SNSF) (Early Postdoc Mobility Fellowship – Project No. P2EZP2_195505). We thank Dr. Milan Gembicky, and Dr. Jake Bailey (U.C. San Diego) for assistance with crystallographic data collection and structure determination. We also thank Dr. Yongxuan Su for mass spectrometry sample analysis at the Molecular Mass Spectrometry Facility at U.C. San Diego. Finally, we thank Conor O'Herin and Alysia Kohlbrand (U.C. San Diego) for expressing and purifying hCAII for use in these studies.

REFERENCES

1. Chen AY; Adamek RN; Dick BL; Credille CV; Morrison CN; Cohen SM Targeting Metalloenzymes for Therapeutic Intervention. Chem. Rev 2019, 119 (2), 1323–1455. [PubMed: 30192523]
2. Cohen SM A Bioinorganic Approach to Fragment-Based Drug Discovery Targeting Metalloenzymes. Acc. Chem. Res 2017, 50 (8), 2007–2016. [PubMed: 28715203]
3. Thornber CW Isosterism and molecular modification in drug design. Chem. Soc. Rev 1979, 8 (4), 563.
4. Ballatore C; Huryn DM; Smith AB Carboxylic Acid (Bio)Isosteres in Drug Design. ChemMedChem 2013, 8 (3), 385–395. [PubMed: 23361977]
5. Dick BL; Cohen SM Metal-Binding Isosteres as New Scaffolds for Metalloenzyme Inhibitors. Inorg. Chem 2018, 57 (15), 9538–9543. [PubMed: 30009599]
6. Dick BL; Patel A; Cohen SM Effect of heterocycle content on metal binding isostere coordination. Chem. Sci 2020, 11 (26), 6907–6914. [PubMed: 33209243]
7. Seo H; Prosser KE; Kalaj M; Karges J; Dick BL; Cohen SM Evaluating Metal–Ligand Interactions of Metal-Binding Isosteres Using Model Complexes. Inorg. Chem 2021, 60 (22), 17161–17172. [PubMed: 34699201]
8. Song Y.n.; Xu H; Chen W; Zhan P; Liu X 8-Hydroxyquinoline: a privileged structure with a broad-ranging pharmacological potential. Med Chem. Commun 2015, 6 (1), 61–74.
9. Gupta R; Luxami V; Paul K Insights of 8-hydroxyquinolines: A novel target in medicinal chemistry. Bioorg. Chem 2021, 108, 104633. [PubMed: 33513476]
10. Jacobsen JA; Fullagar JL; Miller MT; Cohen SM Identifying Chelators for Metalloprotein Inhibitors Using a Fragment-Based Approach. J. Med. Chem 2011, 54 (2), 591–602. [PubMed: 21189019]
11. Chen C; Yang X; Fang H; Hou X Design, synthesis and preliminary bioactivity evaluations of 8-hydroxyquinoline derivatives as matrix metalloproteinase (MMP) inhibitors. Eur. J. Med. Chem 2019, 181, 111563. [PubMed: 31415980]
12. Hopkinson RJ; Tumber A; Yapp C; Chowdhury R; Aik W; Che KH; Li XS; Kristensen JBL; King ONF; Chan MC; Yeoh KK; Choi H; Walport LJ; Thinnes CC; Bush JT; Lejeune C; Rydzik AM; Rose NR; Bagg EA; McDonough MA; Krojer TJ; Yue WW; Ng SS; Olsen L; Brennan PE; Oppermann U; Müller S; Klose RJ; Ratcliffe PJ; Schofield CJ; Kawamura A 5-Carboxy-8-hydroxyquinoline is a broad spectrum 2-oxoglutarate oxygenase inhibitor which causes iron translocation. Chem. Sci 2013, 4 (8), 3110–3117. [PubMed: 26682036]
13. King ONF; Li XS; Sakurai M; Kawamura A; Rose NR; Ng SS; Quinn AM; Rai G; Mott BT; Beswick P; Klose RJ; Oppermann U; Jadhav A; Heightman TD; Maloney DJ; Schofield CJ; Simeonov A Quantitative High-Throughput Screening Identifies 8-Hydroxyquinolines as Cell-Active Histone Demethylase Inhibitors. PLOS ONE 2010, 5 (11), e15535. [PubMed: 21124847]
14. Hanaya K; Suetsugu M; Saijo S; Yamato I; Aoki S Potent inhibition of dinuclear zinc(II) peptidase, an aminopeptidase from Aeromonas proteolytica, by 8-quinolinol derivatives: inhibitor design based on Zn^{2+} fluorophores, kinetic, and X-ray crystallographic study. J. Biol. Inorg. Chem 2012, 17 (4), 517–529. [PubMed: 22311113]
15. Rbaa M; Abousalem AS; Rouifi Z; Benkaddour R; Dohare P; Lakhrissi M; Warad I; Lakhrissi B; Zarrouk A Synthesis, antibacterial study and corrosion inhibition potential of newly synthesis oxathiolan and triazole derivatives of 8-hydroxyquinoline: Experimental and theoretical approach. Surf. Interfaces 2020, 19, 100468.

16. Krawczyk M; Pastuch-Gawolek G; Mrozek-Wilczkiewicz A; Kuczak M; Skonieczna M; Musiol R Synthesis of 8-hydroxyquinoline glycoconjugates and preliminary assay of their β1,4-GalT inhibitory and anti-cancer properties. Bioorg. Chem 2019, 84, 326–338. [PubMed: 30530074]

17. Lawung R; Cherdtrakulkiat R; Nabu S; Prachayasittikul S; Isarankura-Na-Ayudhya C; Prachayasittikul V Repositioning of 8-hydroxyquinoline derivatives as a new promising candidate for combating multidrug resistant Neisseria gonorrhoeae. Excli j. 2018, 17, 840–846. [PubMed: 30233282]

18. Prachayasittikul V; Prachayasittikul V; Prachayasittikul S; Ruchirawat S 8-Hydroxyquinolines: a review of their metal chelating properties and medicinal applications. DDDT 2013, 1157. [PubMed: 24115839]

19. Wishart DS; Knox C; Guo AC; Shrivastava S; Hassanali M; Stothanrd P; Chang Z; Woolsey J DrugBank: a comprehensive resource for in silico drug discovery and exploration. Nucleic Acids Res. 2006, 34 (90001), D668–D672. [PubMed: 16381955]

20. Welsch ME; Snyder SA; Stockwell BR Privileged scaffolds for library design and drug discovery. Current Opinion in Chemical Biology 2010, 14 (3), 347–361. [PubMed: 20303320]

21. Vitaku E; Smith DT; Njardarson JT Analysis of the Structural Diversity, Substitution Patterns, and Frequency of Nitrogen Heterocycles among U.S. FDA Approved Pharmaceuticals: Miniperspective. J. Med. Chem 2014, 57 (24), 10257–10274. [PubMed: 25255204]

22. Liang SH; Southon AG; Fraser BH; Krause-Heuer AM; Zhang B; Shoup TM; Lewis R; Volitakis I; Han Y; Greguric I; Bush AI; Vasdev N Novel Fluorinated 8-Hydroxyquinoline Based Metal Ionophores for Exploring the Metal Hypothesis of Alzheimer's Disease. ACS Med. Chem. Lett 2015, 6 (9), 1025–1029. [PubMed: 26396692]

23. Jin GH; Li H; An S; Ryu J-H; Jeon R Design, synthesis and activity of benzothiazole-based inhibitors of NO production in LPS-activated macrophages. Bioorganic Med. Chem. Lett 2010, 20 (21), 6199–6202.

24. Cottyn B; Acher F; Ramassamy B; Alvey L; Lepoivre M; Frapart Y; Stuehr D; Mansuy D; Boucher J-L; Vichard D Inhibitory effects of a series of 7-substituted-indazoles toward nitric oxide synthases: Particular potency of 1H-indazole-7-carbonitrile. Bioorg. Med. Chem 2008, 16 (11), 5962–5973. [PubMed: 18502134]

25. Keough DT; Skinner-Adams T; Jones MK; Ng A-L; Brereton IM; Guddat LW; de Jersey J Lead Compounds for Antimalarial Chemotherapy: Purine Base Analogs Discriminate between Human and P. Falciparum 6-Oxopurine Phosphoribosyltransferases. J. Med. Chem 2006, 49 (25), 7479–7486. [PubMed: 17149876]

26. McGuigan C; Harris SA; Daluge SM; Gudmundsson KS; McLean EW; Burnette TC; Marr H; Hazen R; Condreay LD; Johnson L; De Clercq E; Balzarini J Application of Phosphoramidate Pronucleotide Technology to Abacavir Leads to a Significant Enhancement of Antiviral Potency. J. Med. Chem 2005, 48 (10), 3504–3515. [PubMed: 15887959]

27. Munk SA; Harcourt DA; Arasasingham PN; Burke JA; Kharlamb AB; Manlapaz CA; Padillo EU; Roberts D; Runde E; Williams L; Wheeler LA; Garst ME Synthesis and Evaluation of 2-(Arylamino)imidazoles as α2-Adrenergic Agonists. J. Med. Chem 1997, 40 (1), 18–23. [PubMed: 9016324]

28. Schönherr D; Wollatz U; Haznar-Garbacz D; Hanke U; Box KJ; Taylor R; Ruiz R; Beato S; Becker D; Weitschies W Characterisation of selected active agents regarding pKa values, solubility concentrations and pH profiles by SiriusT3. Eur. J. Pharm. Biopharm 2015, 92, 155–170. [PubMed: 25758123]

29. Tam KY; Takács-Novák K Multi-wavelength spectrophotometric determination of acid dissociation constants: a validation study. Anal. Chim. Acta 2001, 434 (1), 157–167.

30. Slater B; McCormack A; Avdeef A; Comer JE pH-metric log *P*. 4. Comparison of partition coefficients determined by HPLC and potentiometric methods to literature values. J Pharm. Sci 1994, 83 (9), 1280–1283 . [PubMed: 7830244]

31. Kimblin C; Parkin G Comparison of Zinc and Cadmium Coordination Environments in Synthetic Analogues of Carbonic Anhydrase: Synthesis and Structure of {[Pim$^{Pr^i,Bu^t}$]Cd(OH_2)($OClO_3$)}(ClO_4). Inorg. Chem 1996, 35 (24), 6912–6913. [PubMed: 11666864]

32. Puerta DT; Cohen SM Examination of Novel Zinc-Binding Groups for Use in Matrix Metalloproteinase Inhibitors. Inorg. Chem 2003, 42 (11), 3423–3430. [PubMed: 12767177]
33. Puerta DT; Lewis JA; Cohen SM New Beginnings for Matrix Metalloproteinase Inhibitors: Identification of High-Affinity Zinc-Binding Groups. J. Am. Chem. Soc 2004, 126 (27), 8388–8389. [PubMed: 15237990]
34. Verdolino V; Cammi R; Munk BH; Schlegel HB Calculation of pKa Values of Nucleobases and the Guanine Oxidation Products Guanidinohydantoin and Spiroiminodihydantoin using Density Functional Theory and a Polarizable Continuum Model. J. Phys. Chem. B 2008, 112 (51), 16860–16873. [PubMed: 19049279]
35. Lippert B. Multiplicity of metal ion binding patterns to nucleobases. Coord. Chem. Rev 2000, 200–202, 484-516.
36. Kosturko LD; Folzer C; Stewart RF Crystal and molecular structure of a 2:1 complex of 1-methylthymine-mercury(II). Biochemistry 1974, 13 (19), 3949–3952. [PubMed: 4416138]
37. Grehl M; Krebs B Reaction of Model Nucleobases with the Diaqua(bis(N-methylimidazol-2-yl) ketone)platinum(II) Dication. Synthesis and Structure of the Head-to-Tail Isomers of Bis(9-methylguanine-N7)(bis(N-methylimidazol-2-yl) ketone)platinum(II) Perchlorate, Bis(1-methylcytosine-N3)(bis(N-methylimidazol-2-yl) ketone)platinum(II) Perchlorate, Bis(.mu.-1-methylthyminato-N3,O4)bis[(bis(N-methylimidazol-2-yl) ketone)platinum(II)] Perchlorate, and Bis(.mu.-1-methyluracilato-N3,O4)bis[(bis(N-methylimidazol-2-yl) ketone)platinum(II)] Nitrate. Inorg. Chem 1994, 33 (18), 3877–3885.
38. Chen H; Olmstead MM; Maestre MF; Fish RH Bioorganometallic Chemistry. 7. A Novel, Linear, Two-Coordinate Rh(I) Anionic Amide Complex Formed by the Reaction of the Nucleobase, 1-Methylthymine, with the $[(Cp^*Rh)_2(.mu.\text{-}OH)_3]^+$ Cation at pH 10: Molecular Recognition and Electrostatic Interaction within an Organometallic Hydrophobic Cavity. J. Am. Chem. Soc 1995, 117 (35), 9097–9098.
39. Faggiani R; Howard-Lock HE; Lock CJL; Turner MA The reaction of chloro(triphenylphosphine)gold(I) with 1-methylthymine. Can. J. Chem 1987, 65 (7), 1568–1575
40. Frommer G; Mutikainen I; Pesch FJ; Hillgeris EC; Preut H; Lippert B Platinum(II) coordination to N1 and N7,N1 of guanine: cis-DDP model cross-links in the interior and simultaneous cross-links at the periphery and the interior of DNA. Inorg. Chem 1992, 31 (12), 2429–2434.
41. Rombach M; Gelinsky M; Vahrenkamp H Coordination modes of aminoacids to zinc. Inorganica Chim. Acta 2002, 334, 25–33.
42. Fahrni CJ; O'Halloran TV Aqueous Coordination Chemistry of Quinoline-Based Fluorescence Probes for the Biological Chemistry of Zinc. J. Am. Chem. Soc 1999, 121 (49), 11448–11458.
43. Carter KP; Young AM; Palmer AE Fluorescent Sensors for Measuring Metal Ions in Living Systems. Chem. Rev 2014, 114 (8), 4564–4601. [PubMed: 24588137]
44. McRae R; Bagchi P; Sumalekshmy S; Fahrni CJ In Situ Imaging of Metals in Cells and Tissues. Chem. Rev 2009, 109 (10), 4780–4827. [PubMed: 19772288]
45. McGowan JE; Harper AD; Davison EK; Jeong JY; Mros S; Harbison-Price N; Van Zuylen EM; Knottenbelt MK; Heikal A; Ferguson SA; McConnell MA; Cook GM; Krittaphol W; Walker GF; Brimble MA; Rennison D Substituted sulfonamide bioisosteres of 8-hydroxyquinoline as zinc-dependent antibacterial compounds. Bioorg. Med. Chem. Lett 2020, 30 (11), 127110. [PubMed: 32229060]
46. Okamoto K; Kuwabara J; Kanbara T Chemistry of Thioamides; Murai T, Ed.; Springer: Singapore, 2019; pp 157–191.
47. Al-Oudat BA; Jaradat HM; Al-Balas QA; Al-Shar'i NA; Bryant-Friedrich A; Bedi MF Design, synthesis and biological evaluation of novel glyoxalase I inhibitors possessing diazenylbenzenesulfonamide moiety as potential anticancer agents. Bioorg. Med. Chem 2020, 28 (16), 115608. [PubMed: 32690268]
48. Lovejoy B; Welch AR; Carr S; Luong C; Broka C; Hendricks RT; Campbell JA; Walker KA; Martin R; Van Wart H; Browner MF Crystal structures of MMP-1 and -13 reveal the structural basis for selectivity of collagenase inhibitors. Nat. Struct. Biol 1999, 6 (3), 217–21. [PubMed: 10074939]

49. Eriksson AE; Jones TA; Liljas A Refined structure of human carbonic anhydrase II at 2.0 A resolution. Proteins 1988, 4 (4), 274–282. [PubMed: 3151019]
50. Sellin S; Eriksson LE; Aronsson AC; Mannervik B Octahedral metal coordination in the active site of glyoxalase I as evidenced by the properties of Co(II)-glyoxalase I. J. Biol. Chem 1983, 258 (4), 2091–2093. [PubMed: 6296126]
51. Rouffet M; de Oliveira CAF; Udi Y; Agrawal A; Sagi I; McCammon JA; Cohen SM From Sensors to Silencers: Quinoline- and Benzimidazole-Sulfonamides as Inhibitors for Zinc Proteases. J. Am. Chem. Soc 2010, 132 (24), 8232–8233. [PubMed: 20507095]
52. Tanakit A; Rouffet M; Martin DP; Cohen SM Investigating chelating sulfonamides and their use in metalloproteinase inhibitors. Dalton Trans. 2012, 41 (21), 6507–6515. [PubMed: 22411188]
53. Ekinci D; Çavdar H; Durdagi S; Talaz O; Şentürk M; Supuran CT Structure–activity relationships for the interaction of 5,10-dihydroindeno[1,2-b]indole derivatives with human and bovine carbonic anhydrase isoforms I, II, III, IV and VI. Eur. J. Med. Chem 2012, 49, 68–73. [PubMed: 22245047]
54. Awadallah FM; Bua S; Mahmoud WR; Nada HH; Nocentini A; Supuran CT Inhibition studies on a panel of human carbonic anhydrases with N1-substituted secondary sulfonamides incorporating thiazolinone or imidazolone-indole tails. J. Enzyme Inhib. Med. Chem 2018, 33 (1), 629–638. [PubMed: 29536779]
55. Bonardi A; Nocentini A; Bua S; Combs J; Lomelino C; Andring J; Lucarini L; Sgambellone S; Masini E; McKenna R; Gratteri P; Supuran CT Sulfonamide Inhibitors of Human Carbonic Anhydrases Designed through a Three-Tails Approach: Improving Ligand/Isoform Matching and Selectivity of Action. J. Med. Chem 2020, 63 (13), 7422–7444. [PubMed: 32519851]
56. Carta F; Di Cesare Mannelli L; Pinard M; Ghelardini C; Scozzafava A; McKenna R; Supuran CT A class of sulfonamide carbonic anhydrase inhibitors with neuropathic pain modulating effects. Bioorg. Med. Chem 2015, 23 (8), 1828–1840. [PubMed: 25766630]
57. Puerta DT; Cohen SM Elucidating Drug-Metalloprotein Interactions with Tris(pyrazolyl)borate Model Complexes†. Inorg. Chem 2002, 41 (20), 5075–5082. [PubMed: 12354040]
58. Schönherr D; Wollatz U; Haznar-Garbacz D; Hanke U; Box KJ; Taylor R; Ruiz R; Beato S; Becker D; Weitschies W Characterisation of selected active agents regarding pKa values, solubility concentrations and pH profiles by SiriusT3. Eur. J. of Pharm. Biopharm 2015, 92, 155–170. [PubMed: 25758123]
59. Slater B; McCormack A; Avdeef A; Comer JEA PH-Metric logP.4. Comparison of Partition Coefficients Determined by HPLC and Potentiometric Methods to Literature Values. J. Pharm. Sci 1994, 83 (9), 1280–1283. [PubMed: 7830244]
60. Avdeef A; Box KJ; Comer JE; Gilges M; Hadley M; Hibbert C; Patterson W; Tam KY PH-metric log P 11. pKa determination of water-insoluble drugs in organic solvent-water mixtures. J. Pharm. Biomed. Anal 1999, 20 (4), 631–41. [PubMed: 10704132]
61. Chiba T; Ohwada J; Sakamoto H; Kobayashi T; Fukami TA; Irie M; Miura T; Ohara K; Koyano H Design and evaluation of azaindole-substituted N-hydroxypyridones as glyoxalase I inhibitors. Bioorganic Med. Chem. Lett 2012, 22 (24), 7486–7489.
62. Monnard FW; Nogueira ES; Heinisch T; Schirmer T; Ward TR Human carbonic anhydrase II as host protein for the creation of artificial metalloenzymes: the asymmetric transfer hydrogenation of imines. Chem. Sci 2013, 4 (8), 3269–3274.

Synopsis

Metal-binding isosteres (MBIs) of 8-hydroxyquinoline (8-HQ) were designed and their coordination chemistry was study using a bioinorganic model system [($Tp^{Ph,Me}$Zn(MBI)] ($Tp^{Ph,Me}$ = hydrotris(3,5-phenylmethylpyrazolyl)borate). The MBIs cover a wide range of physiochemical properties, while retaining inhibition activity against Zn(II)-dependent metalloenzymes. The results demonstrate the utility of 8-HQ MBIs as a starting scaffold for metalloenzyme inhibitor development.

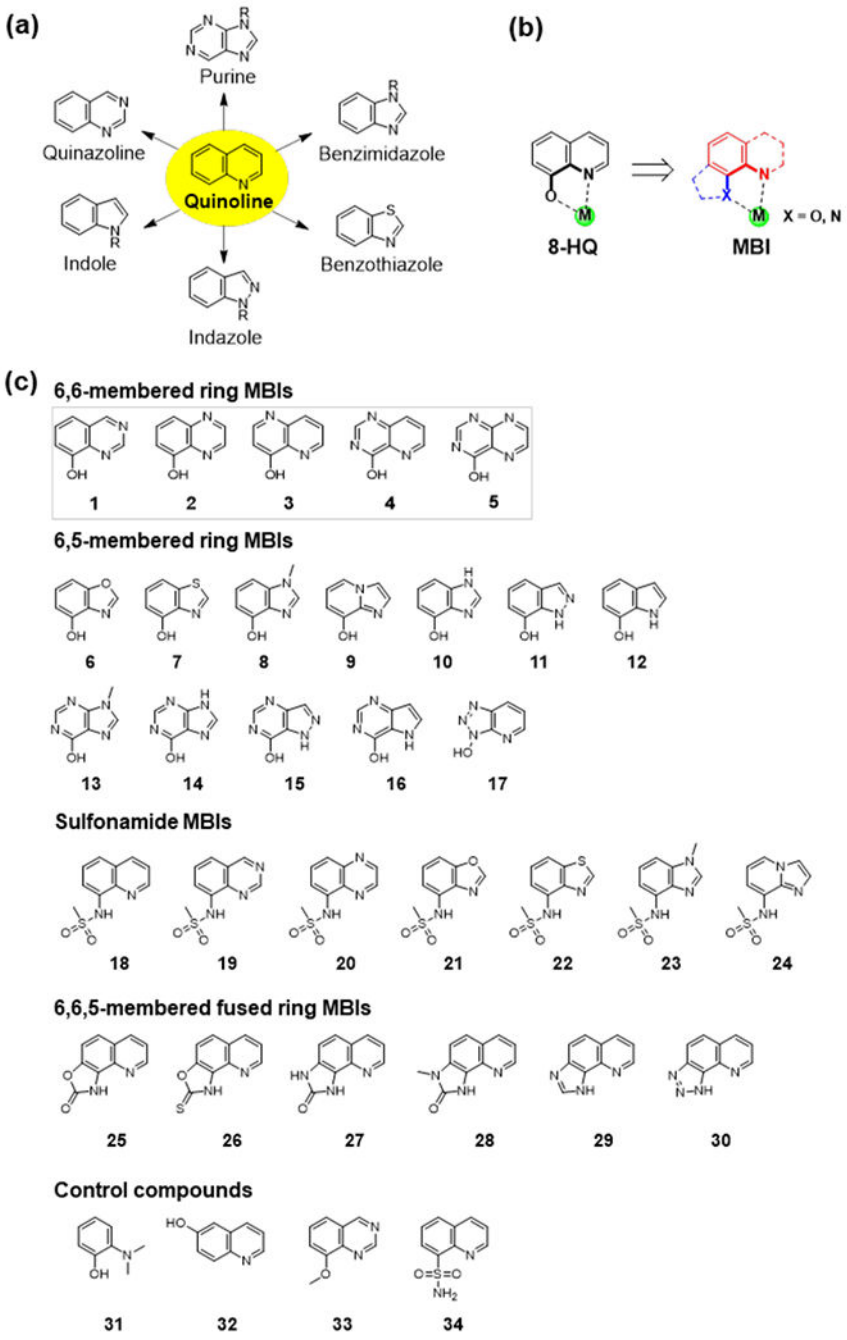

Figure 1.

(a) Quinoline and examples of its isosteres that are frequently used in drug discovery. (b) The hydroxyl group (blue) and the quinoline ring scaffold (red) were replaced with various isosteres. (c) Library of 8-HQ MBIs.

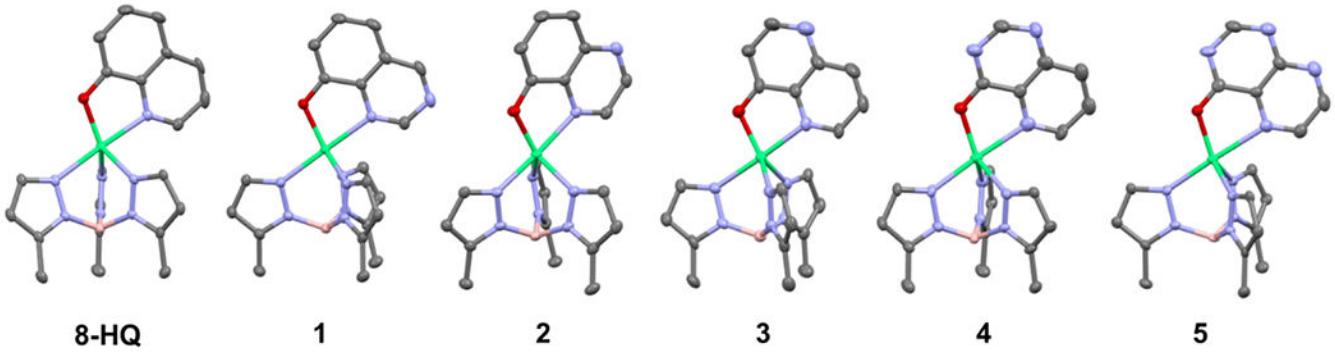

Figure 2.

Crystal structure of [$Tp^{Ph,Me}$Zn(**MBI**)] complexes with 6,6-membered ring MBIs. (ORTEP, 50% probability ellipsoids). Hydrogen atoms and phenyl groups from the $Tp^{Ph,Me}$ ligand were removed for clarity. Color scheme: carbon = gray, nitrogen = blue, oxygen = red, boron = pink, and zinc = green.

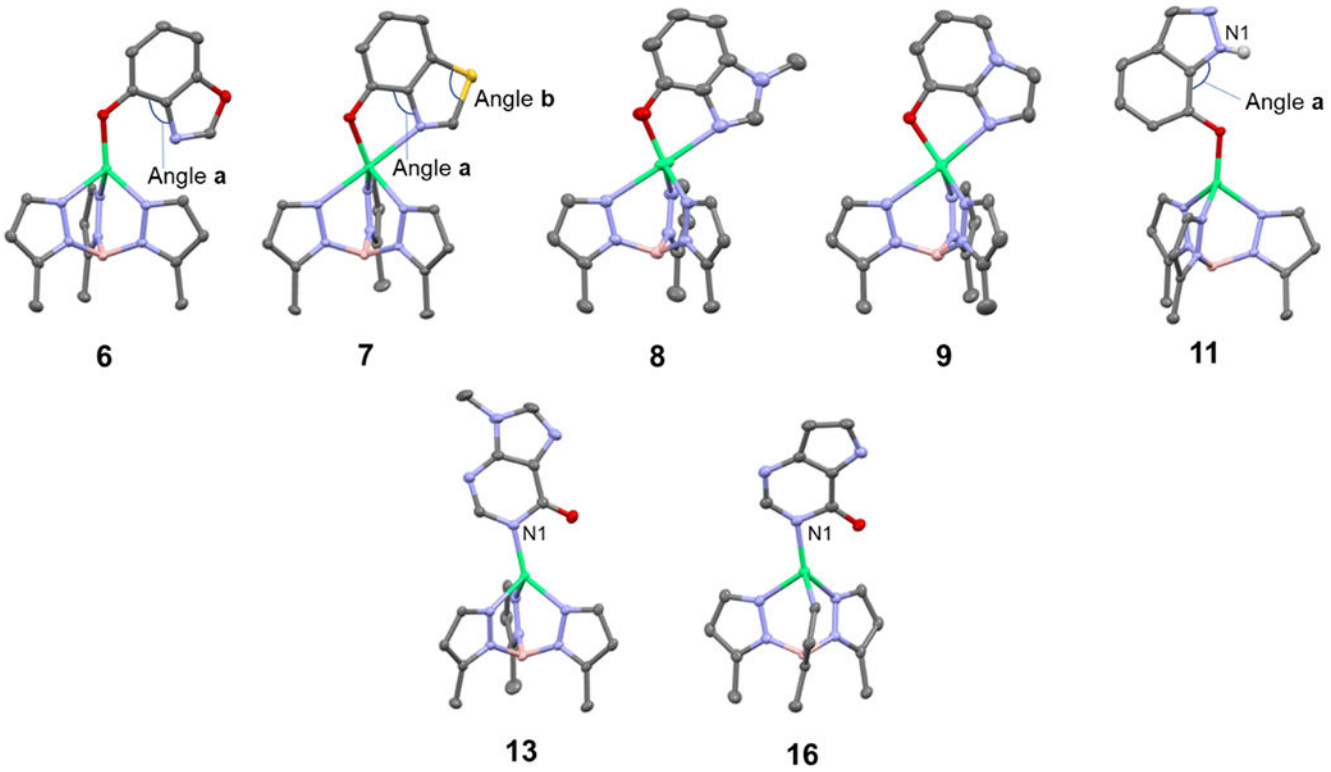

Figure 3.

Crystal structure of [Tp^{Ph,Me}Zn(**MBI**)] complexes with 6,5-membered ring MBIs. (ORTEP, 50% probability ellipsoids). Angle **a** is defined between the 5- and 6-membered ligand rings and angles **a** and **b** together are used to describe overall internal ligand geometry on the binding modes of MBI **6**, **7**, and **11**. N1 is labeled to indicate the NH group on MBI **11** and the nitrogen atom providing monodentate coordination of MBI **13** and **16**. Hydrogen atoms and phenyl groups from the Tp^{Ph,Me} ligand were removed for clarity. Color scheme: carbon = gray, nitrogen = blue, oxygen = red, sulfur = yellow, boron = pink, and zinc = green.

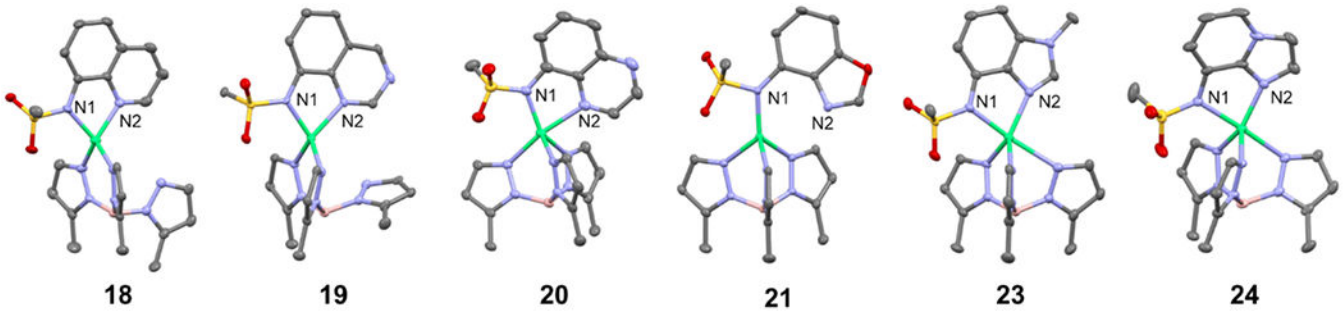

Figure 4.

Crystal structure of [$Tp^{Ph,Me}$Zn(**MBI**)] complexes with sulfonamide MBIs. (ORTEP, 50% probability ellipsoids). N1 and N2 are labeled to identify nitrogen atoms that are position to participate in bidentate coordination to Zn(II) center. Hydrogen atoms and phenyl groups from the $Tp^{Ph,Me}$ ligand were removed for clarity. Color scheme: carbon = gray, nitrogen = blue, oxygen = red, sulfur = yellow, boron = pink, and zinc = green.

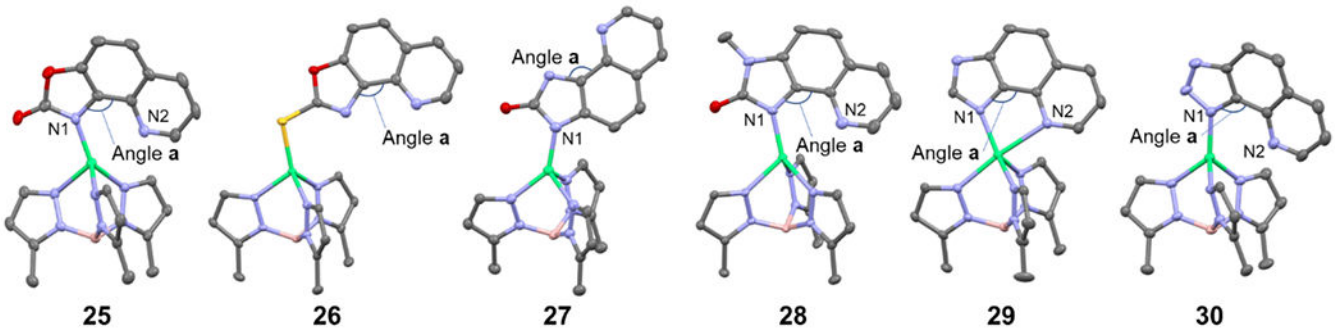

Figure 5.

Crystal structure of [$Tp^{Ph,Me}$Zn(**MBI**)] complexes with 6,6,5-membered ring MBIs. (ORTEP, 50% probability ellipsoids). Angle **a** makes is defined between the 5- and 6-membered ligand rings and is used to describe overall internal ligand geometry on the binding modes of the MBIs. N1 and N2 are labeled to identify nitrogen atoms that are positioned to participate in bidentate coordination to Zn(II) center. Hydrogen atoms and phenyl groups from the $Tp^{Ph,Me}$ ligand were removed for clarity. Color scheme: carbon = gray, nitrogen = blue, oxygen = red, sulfur = yellow, boron = pink, and zinc = green.

Table 1.

Measured and calculated pK_a and log$P/D_{7.4}$ values of 8-HQ MBI library. pK_a values were measured in the range of pH 2.0 – 12.0. All pK_a and log$P$ experiments yielded standard deviations <0.05. Calculated pK_a and log$P/D_{7.4}$ values were obtained using Marvin (ChemAxon) software package. Published pK_a values can be found in the Supporting Information (Table S3).

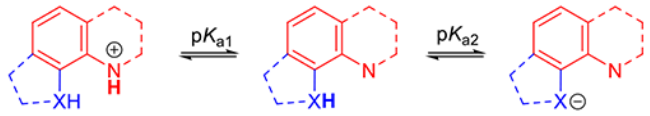

MBI	Measured			Calculated		
	pK_a	log$P$	log$D_{7.4}$	pK$_a$	log$P$	log$D_{7.4}$
8-HQ	4.97, 9.62	1.86	1.85	4.83, 9.36	1.83	1.82
1	3.38, 8.55	−0.1	−0.13	1.66, 9.03	1.12	1.11
2	8.69	0.93	0.90	2.39, 8.31	1	0.95
3	3.04, 9.50	0.53	0.52	2.99, 13.57	1	0.99
4	2.44, 8.90	−0.52	−0.53	1.51, 11.44	0.88	0.88
5	7.64	−0.6	−0.80	10.65	−0.01	−0.01
6	8.40	1.22	1.18	7.85	1.02	0.89
7	8.74	1.86	1.84	1.61, 8.16	1.81	1.74
8	4.61, 9.30	0.71	0.70	4.82, 8.25	1.18	1.11
9	5.43, 9.29	−0.11	−0.12	5.48, 8.12	0.76	0.38
10	5.28, 8.88	0.68	0.67	5.19, 8.28	0.96	0.88
11	8.37	1.68	1.64	1.08, 8.21	0.99	0.99
12	9.43	1.56	1.56	9.61	1.77	1.77
13	9.17	−0.30	−0.31	2.79, 10.96	0.22	0.22
14	8.81	−1.4	−1.42	2.28, 9.41	−0.01	−0.01
16	2.88, 10.01	0.82	−2.46	0.07, 12.97	0.83	0.83
17	3.34	0.23	−3.83	4.98	−0.22	−2.32
18	3.17, 8.97	1.01	0.99	3.7, 7.25	0.5	0.18
19	8.25	0.23	0.17	1.96, 7.19	−0.2	−0.55
20	2.16, 8.11	0.49	0.41	2.35, 7.15	−0.33	−0.69
21	7.81	0.37	0.23	0.04, 6.97	−0.31	−0.76
22	8.18	1.23	1.16	2.09, 7.1	0.49	0.1
23	4.45, 8.67	0.69	0.67	5.26, 7.18	−0.14	−0.55
24	4.56, 8.34	−0.34	−0.39	5.97, 8.06	−0.87	−1.02
25	8.27	1.49	1.44	4.02, 8.93	1.49	1.48
26	6.45	1.21	0.22	2.41, 5.32	1.53	0.2
27	10.92	1.56	1.56	3.04, 12.09	1.3	1.3
29	4.92, 11.75	1.97	1.97	2.73, 12.01	1.42	1.41
30	7.27	1.59	1.23	1.41, 7.37	1.46	1.15

Table 2.

Selected bond lengths and angles of [$Tp^{Ph,Me}$Zn(**MBI**)] complexes with 6,6-membered ring MBIs.

MBI	Binding Mode	Zn-O (Å)	Zn-N (Å)	O-Zn-N (°)	Tau, τ_5 (°)
8-HQ	Bidentate	1.9497(10)	2.1865(12)	80.68(5)	0.73
1	Bidentate	1.9590(13)	2.1893(16)	80.59(6)	0.72
		1.9552(13)	2.1938(16)	80.84(6)	0.71
2	Bidentate	1.947(3)	2.220(4)	79.77(12)	0.66
		1.944(3)	2.201(3)	79.65(13)	0.67
3	Bidentate	1.958(5)	2.239(6)	78.6(2)	0.73
		1.957(5)	2.217(6)	80.1(2)	0.74
4	Bidentate	1.971(6)	2.289(8)	76.5(3)	0.68
		1.960(6)	2.255(7)	78.5(2)	0.74
5	Bidentate	1.979(8)	2.363(10)	76.6(3)	0.71
		1.971(8)	2.407(10)	76.1(3)	0.68

Table 3.

Selected bond lengths and angles of [$Tp^{Ph,Me}$Zn(**MBI**)] complexes with 6,5-membered ring MBIs.

MBI	Binding Mode	Zn-O (Å)	Zn-N (Å)	O-Zn-N (°)	Angle a and b (°)	Tau (°)
8-HQ	Bidentate	1.9497(10)	2.1865(12)	80.68(5)	116.30(14), 122.19(15)	τ_5, 0.73
6	Monodentate	1.8930(17)	-	-	129.29(19), 103.55(16)	τ_4, 0.76
7	Bidentate	1.9417(11)	2.2792(13)	81.22(5)	120.48(13), 90.00(8)	τ_5, 0.72
8	Bidentate	1.932(2)	2.292(3)	83.32(10)	124.3(3), 106.7(3)	τ_5, 0.79
		1.918(2)	2.340(3)	82.30(10)	124.3(3), 107.1(3)	τ_5, 0.72
9	Bidentate	1.9612(15)	2.1899(17)	83.40(6)	125.24(19), 105.9(2)	τ_5, 0.54
11	Monodentate	1.8766(12)	-	-	130.28(17), 112.11(17)	τ_4, 0.79

Table 4.

Selected bond lengths and angles of $Tp^{Ph,Me}Zn(MBI)$ complexes with 6,6,5-membered fused ring MBIs.

MBI	Binding Mode	Zn-N1 (Å)	Zn-N2 (Å)	N1-Zn-N2 (°)	Angle a (°)	Tau (°)
25	Monodentate	1.9438(18)	2.621[c]	75.73[c]	127.1(2)	τ_4, 0.72
26	Monodentate	2.2505(6)[a]	-	-	131.8(2)	τ_4, 0.76
27	Monodentate	1.910(3)[b]	-	-	131.4(3)	τ_4, 0.72
28	Monodentate	1.9486(14)	2.811[c]	72.584[c]	128.42(15)	τ_4, 0.72
29	Bidentate	1.9779(14)	2.4413(14)	79.68(5)	126.55(15)	τ_5, 0.54
30	Monodentate	1.934(2)	2.933[c]	71.21[c]	129.9(2)	τ_4, 0.74

[a] Zn-S bond distance.

[b] Zn-external nitrogen bond distance.

[c] Not bound to the Zn(II) center, measured values based on X-ray crystallographic data.

Table 5.

Percent inhibition values of 8-HQ MBIs (200 μM) against MMP-2, GLO1, and hCAII. Standard deviations from triplicate measurements are given in parentheses. Cells are color-coded by percent inhibition: white (<20%), yellow (20–50%), and red (>50%). Black cells were compounds that interfered with the assay due to the poor solubility under the assay condition.

MBI	MMP-2	GLO1	hCAII
8-HQ	57 (3)	95 (6)	<5
1	32 (3)	95 (7)	<5
2	34 (2)	37 (5)	<5
3	39 (3)	<5	<5
4		6 (4)	<5
5	34 (5)	10 (5)	<5
6	7 (5)	22 (4)	37 (4)
7	<5	27 (4)	<5
8	7 (5)	23 (7)	44 (8)
9	6 (9)	41 (4)	<5
10	<5	44 (7)	<5
11	<5	77 (1)	<5
12	17 (7)	30 (5)	89 (2)
13		36 (7)	<5
14		7 (9)	<5
15	6 (6)	<5	<5
16	<5	13 (5)	18 (5)
17	20 (3)	<5	<5
18	59 (2)	95 (1)	<5
19	13 (5)	87 (4)	51 (6)
20	12 (5)	63 (8)	9 (6)
21	<5	<5	<5
22	<5	<5	<5
23	<5	<5	<5
24	<5	60 (9)	11 (9)
25	7 (5)	<5	
26	41 (3)	50 (13)	6 (8)
27	9 (5)	31 (10)	<5
28	6 (4)	<5	63 (2)
29	<5	65 (9)	<5
30	<5	<5	
31	<5	36 (3)	<5
32	26 (7)	<5	N/A
33	6 (11)	78 (5)	N/A

MBI	MMP-2	GLO1	hCAII
34	9 (5)	<5	<5